Discover Oncology

Research

Predictive value of combined DCE-MRI perfusion parameters and clinical features nomogram for microsatellite instability in colorectal cancer

Leping Peng[1] · Wenting Ma[2] · Xiuling Zhang[1] · Fan Zhang[1] · Fang Ma[1] · Kai Ai[3] · Xiaomei Ma[2] · Yingmei Jia[2] · Hong Ou-Yang[2] · Shengting Pei[2] · Tao Wang[4] · Yuanhui Zhu[2] · Lili Wang[2]

Received: 20 January 2025 / Accepted: 13 May 2025
Published online: 23 May 2025

Abstract

Objectives To develop a nomogram that combines dynamic contrast-enhanced magnetic resonance imaging (DCE-MRI) perfusion parameters, ADC values and clinical features to preoperatively identify microsatellite instability (MSI) in patients with colorectal cancer (CRC).

Methods This retrospective study included 63 CRC patients who underwent preoperative DCE-MRI and had immunohistochemistry results available. Two radiologists, in a double-blind manner, placed two circular regions of interests in the area with the highest perfusion intensity on the DCE-MRI perfusion map and the corresponding area on the ADC map. Perfusion parameters and ADC values were measured, and the average values from both radiologists were used for subsequent analysis. Univariate analysis was performed to identify independent risk factors for MSI. A nomogram was then constructed by combining the most significant clinical risk factors with DCE-MRI perfusion parameters. The model's performance was evaluated using receiver operating characteristic (ROC) curves. Calibration curves, decision curve analysis (DCA), and clinical impact curves (CIC) were used to assess the nomogram's clinical utility and net benefit.

Results The nomogram prediction model, which combined PLT, LNM, K^{trans}, K_{ep}, iAUC, and ADC, demonstrated good predictive performance. The combined model had an AUC of 0.951 (95% CI: 0.903–0.998), an accuracy of 0.873, a sensitivity of 1.000, and a specificity of 0.818. Both the DCA and CIC demonstrated good clinical applicability and net benefit.

Conclusion The nomogram method demonstrated good potential in the preoperative individualized identification of MSI status in CRC patients. This tool can assist clinicians in adopting appropriate treatment strategies and optimizing personalized stratification for CRC patients.

Keywords Magnetic resonance imaging · DCE · Nomogram · Microsatellite instability · Colorectal cancer

Leping Peng and Wenting Ma are the authors contributed equally as first authors; Yuanhui Zhu and Lili Wang contributed equally to this work and serve as co-corresponding authors.

Supplementary Information The online version contains supplementary material available at https://doi.org/10.1007/s12672-025-02705-x.

✉ Yuanhui Zhu, zyh960419@163.com; ✉ Lili Wang, wanglilihq@163.com; Leping Peng, p13517993320@163.com; Wenting Ma, 384413759@qq.com | [1]Gansu University of Chinese Medicine, Lanzhou 730000, Gansu, China. [2]Department of Radiology, Gansu Provincial Hospital, Lanzhou 730000, Gansu, China. [3]Department of Clinical and Technical Support, Philips Healthcare, Xi'an 710065, Shanxi, China. [4]Department of Colorectal Surgery, Gansu Provincial Hospital, Lanzhou 730000, Gansu, China.

1 Introduction

According to the 2022 GLOBOCAN statistics from the International Agency for Research on Cancer (IARC), colorectal cancer (CRC) is the third most common malignancy worldwide, with 1.966 million new cases and 904,000 deaths [1]. CRC is a highly heterogeneous gastrointestinal malignancy driven by epigenetic mechanisms [2]. The progression mechanism of CRC involves gene mutations in tumor cells, immune evasion, and changes in the tumor microenvironment. Among these, CRCs with high microsatellite instability (MSI-H) exhibit a range of distinctive biological behaviors, including increased immune cell infiltration, enhanced angiogenesis, and fewer lymph node metastases [3]. Additionally, patients with MSI-H CRC do not benefit from adjuvant chemotherapy with pyrimidine analogs or fluorouracil [4, 5]. Based on the unique biological characteristics of MSI-H in CRC, critical diagnostic and therapeutic strategies can be implemented in clinical practice, such as combining neoadjuvant immunotherapy, neoadjuvant chemoradiotherapy, and targeted therapies. The Chinese Society of Clinical Oncology guidelines for CRC diagnosis and treatment [6], the National Comprehensive Cancer Network guidelines [7], and the European Society for Medical Oncology guidelines [8] recommend universal MSI/dMMR testing for all CRC patients.

Currently, the determination of MSI status primarily relies on histopathological specimen collection and molecular biological techniques, such as immunohistochemistry (IHC) staining and polymerase chain reaction (PCR) [9]. However, these invasive histological methods have limitations, including subjectivity in sample selection and invasiveness. Moreover, the availability of MSI testing is often restricted to advanced medical institutions and is expensive. More importantly, due to the spatiotemporal heterogeneity of tumors, the expression levels of MMR proteins detected in different biopsy sites may be either underestimated or overestimated [10]. Therefore, seeking a comprehensive and non-invasive method for preoperatively predicting MSI-H status is crucial for clinical diagnosis and treatment.

DCE-MRI, as a functional imaging technique, has been widely applied in clinical practice. By quantifying parameters related to tumor microvascular angiogenesis, perfusion, and permeability, DCE-MRI reflects changes in the microvascular system within tumor tissue in terms of hemodynamics and morphology [11]. Additionally, the ADC calculated from diffusion-weighted imaging (DWI) can reveal the diffusion properties of water molecules within tumors [12]. Multiple studies [13–15] have demonstrated that ADC values are closely associated with the preoperative staging, malignancy, and prognosis of CRC. Therefore, DCE-MRI parameters and ADC values may more effectively reflect the MSI status of CRC. To our knowledge, existing DCE-MRI studies have primarily focused on evaluating the efficacy, prognosis, lymph node staging, and predicting extramural vascular invasion in CRC [16–20]. However, few studies have explored the utility value of DCE-MRI parameters and ADC values in the quantitatively predicting the MSI status of CRC.

Radiogenomics is an emerging interdisciplinary technology that combines medical imaging techniques with genomics. It aims to explore the correlations between imaging features (such as tumor morphology, texture, and density) and genomic and molecular characteristics (such as mutation status and molecular subtypes) [21]. This approach not only helps to infer the biological mechanisms of diseases and deepen the understanding of overall phenotypes but also enables the identification of macroscopic imaging biomarkers that can predict genomic characteristics. As a result, radiogenomics facilitates non-invasive diagnosis, prognostic evaluation, and treatment monitoring of complex diseases. In this study, we aimed to develop a nomogram model that integrates DCE-MRI parameters, ADC values, and clinical features to assess the MSI status of CRC patients. This study represents a simple application of radiogenomics, using imaging parameters to indirectly reflect the molecular characteristics of tumors. It further demonstrates the potential of imaging data in predicting MSI status.

2 Materials and methods

2.1 Patients and data collection

This study was approved by the Ethics Committee of Gansu Provincial Hospital (no. 2023-725), and the requirement for informed consent was waived. We retrospectively collected data from patients diagnosed with CRC through postoperative pathological biopsy between May 2021 and January 2024. All patients underwent DCE-MRI scans of the abdomen, along with conventional sequence scans, prior to surgery. Inclusion criteria: (1) Patients diagnosed

with CRC through postoperative pathology; (2) DCE-MRI examination conducted within one month prior to surgery; (3) Postoperative PCR testing for MSI status is available. Exclusion criteria: (1) Patients who received any anticancer treatment (including radiotherapy, chemotherapy, or immunotherapy) prior to the MRI examination; (2) Poor image quality or significant artifacts; (3) Incomplete or unavailable clinical data; (4) Tumor not visible on MRI images.

Clinical and pathological information was collected from medical records, including age, sex, tumor location (rectum, left colon, right colon), serous/mesangial layer invasion, Degree of differentiation, Morphological classification, platelet count (PLT), carcinoembryonic antigen (CEA), carbohydrate antigen 19-9 (CA19-9), carbohydrate antigen 7–24 (CA7-24), high-density lipoprotein (HDL), and low-density lipoprotein (LDL).

2.2 MRI imaging

All patients underwent routine abdominal and pelvic MRI scans using one of two MRI scanners; the 3.0 T MRI scanner [(Elition, Philips Healthcare, the Netherlands) and (Siemens Skyra, Germany)], with phased-array multichannel torso coils. The ADC images were automatically generated from the DWI sequence (b = 0, 1000 s/mm^2). The T1-weighted DCE-MRI scanning commenced immediately after the intravenous administration of a contrast agent at a rate of 3.5 mL/s, with a dose of 0.2 mL/kg of body weight, followed by a 20 mL saline flush using an automatic power injector (Urich Tennessee-XD2003, Germany) through the antecubital vein. The parameters of the two MRI scanners are detailed in Table S1.

2.3 Image analysis

All ADC and DCE-MRI images of CRC patients were exported from the Picture Archiving and Communication System (PACS) and saved in DICOM format. To ensure uniform resolution and voxel size across all DCE-MRI images, they were first resampled using linear interpolation. Next, grayscale discretization was normalized by setting a fixed bin size of 5 for absolute grayscale discretization. The processed images were then transferred to the Tissue 4D post-processing workstation (syngo MMWP, VE40 A, Siemens AG) for further analysis. Two radiologists, each with more than 5 years of experience in abdominal imaging diagnosis, independently placed regions of interest (ROIs) on the areas of highest perfusion in DCE-MRI images and the areas of diffusion restriction in ADC maps, using a double-blind method. The system then automatically generated perfusion images and parameter values, as well as ADC values. These parameters included the contrast transfer constant (K^{trans}), the fractional volume of the extracellular space (V_e), the reflux rate between the extracellular space and blood plasma (K_{ep}), and the initial area under the curve in 60 s (iAUC), with iAUC serving as a semi-quantitative perfusion parameter. K^{trans}, K_{ep}, and V_e were considered quantitative perfusion parameters. Two radiologists independently measured the DCE-MRI parameters and repeated the ADC measurements after a 3-week interval. To evaluate the consistency and robustness of their measurements, both radiologists randomly selected 20 patients and re-measured the parameters after a 1-month interval. A Kappa value of ≥ 0.75 was considered to indicate good agreement. The average values of the DCE-MRI parameters and ADC measurements from the two radiologists were then used for further analysis. Figure 1 showed clinical examples of MSI and MSS patients with CRC. Figure 2 illustrated the measurement of imaging parameters, pathological assessment, and the overall process of this study.

2.4 MSI assessment

The MSI status of four mismatch repair (MMR) proteins, including mutL homologue 1 (MLH1), mutS homologue 2 (MSH2), mutS homologue 6 (MSH6), and postmeiotic segregation increased 2 (PMS2), was assessed using the standard streptavidin–biotin–peroxidase procedure. The MMR protein staining results were independently reviewed and confirmed by two pathologists with over 8 years of experience in CRC diagnosis to ensure the accuracy of MSI status assessment (Fig. 2). Based on the expression results of MMR proteins, patients were classified as MSI if any one of the four proteins showed negative staining. Conversely, if all four proteins exhibited positive staining, the patients were classified as MSS [22–24].

2.5 Selection of optimal features and model development

Univariate logistic regression analysis was performed on the collected clinicopathological data to identify independent predictors of MSI status. Independent sample t-tests or Mann–Whitney *U* tests were used to analyze DCE-MRI parameters (K^{trans}, K_{ep}, V_e, and iAUC) and ADC values. Parameters and clinical features with two-tailed *P*-values < 0.05 were included in the model construction. A total of 10 predictive models were established: Clinical_model, K_{ep}_iAUC, K_{ep}_ADC,

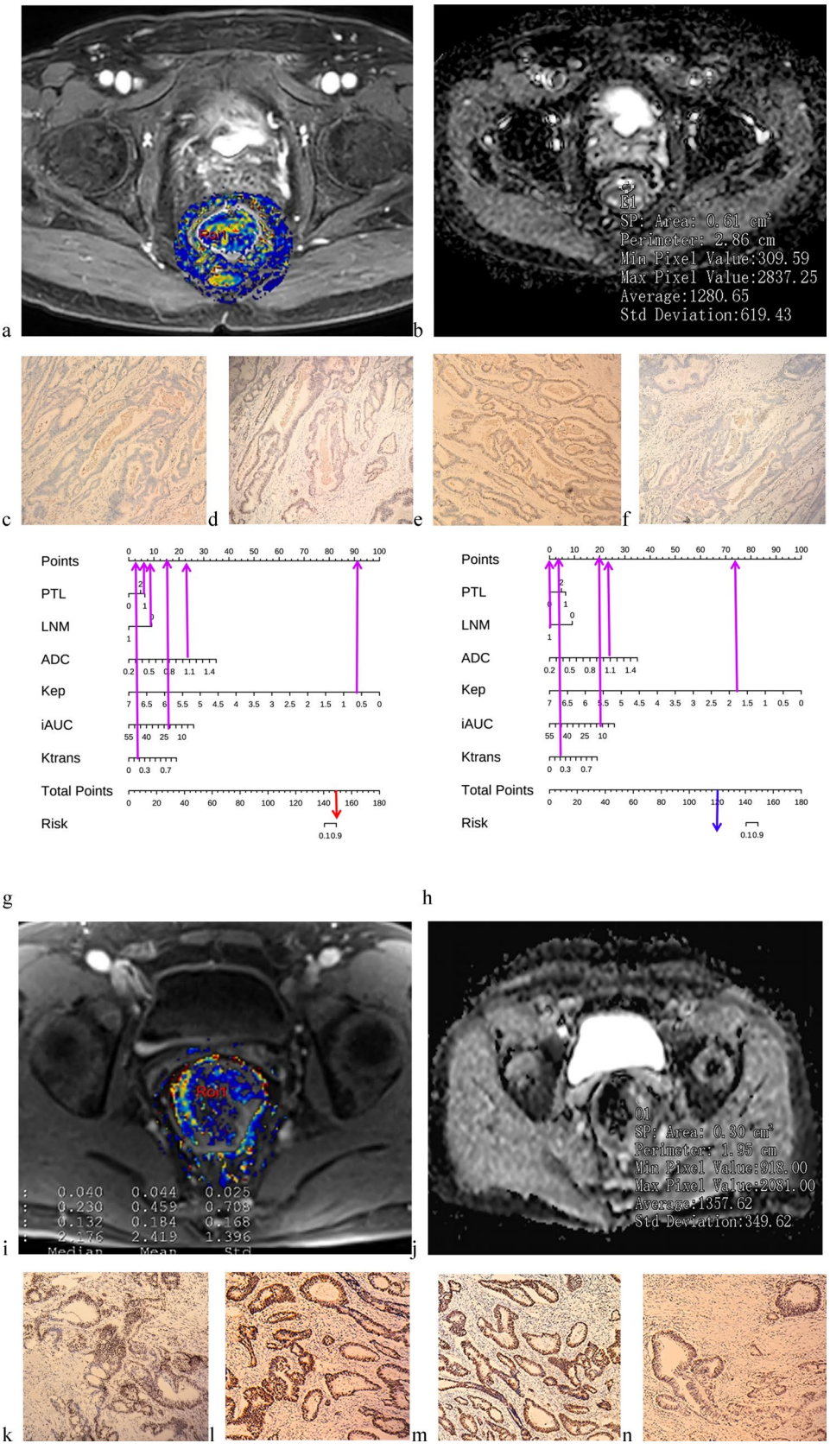

Fig. 1 Case Analysis of MSI and MSS Patients in Clinical Applications. A 73-year-old man with rectal cancer, immunohistochemical staining exhibited MSI (**a**–**g**), and a 53-year-old man with rectal cancer, immunohistochemical staining exhibited MSS (**h**–**n**); **a** and **i** ROI_1 in DCE-MRI perfusion maps. **b** and **j** ROI_2 in ADC maps; **c**–**f** immunohistochemical test results in the MSI patient [**c**, MLH1(–); **d**, MSH2(+); **e**, MSH6(+); **f**, PMS2(–)]and **k**–**n** immunohistochemical test results in the MSS patient [k, MLH1(+); l, MSH2(+); m, MSH6(+); n, PMS2(+)]; the total nomogram scores for MSI and MSS patients in **g** and **h** were 148 and 120, respectively, predicting MSI risk greater than 0.9 and less than 0.1, respectively

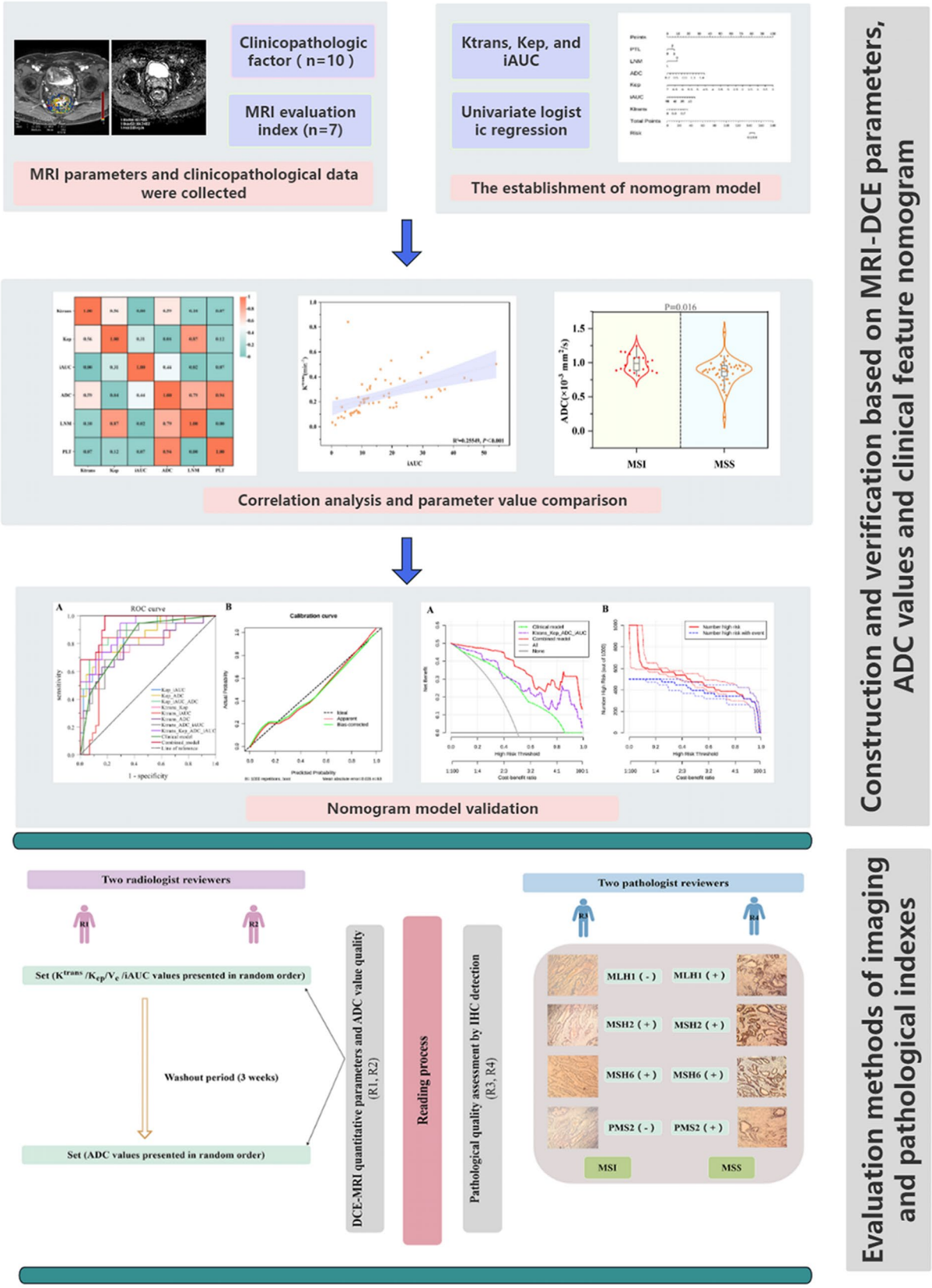

Fig. 2 The overall framework, imaging parameters, and the process of pathological assessment of this study. *ADC* apparent diffusion coefficient, *DCE* dynamic contrast-enhanced, *IHC* immunohistochemistry

K_{ep}_iAUC_ADC, K^{trans}_K_{ep}, K^{trans}_iAUC, K^{trans}_ADC, K^{trans}_ADC_iAUC, K^{trans}_K_{ep}_ADC_iAUC, and K^{trans}_K_{ep}_ADC_iAUC_Clinical (hereafter referred to as Combined_model). The nomogram model was presented in a visualized format.

2.6 Evaluation of nomogram performance and clinical application

The goodness of fit for the nomogram was evaluated using the calibration curve (Hosmer–Lemeshow H test), while the predictive ability of the 10 models was assessed through receiver operating characteristic (ROC) curves and DeLong test. Bootstrap analysis with 1000 iterations was conducted to assess potential biases in the proposed models. Clinical decision curve analysis (DCA) and clinical impact curves (CIC) were employed to assess their clinical applicability and net benefit. Spearman and Pearson correlation tests were used to evaluate the relationships between optimal clinical features and the values of DCE-MRI parameters and ADC values, which were visualized using a correlation heatmap. Additionally, differences in DCE-MRI parameters and ADC values between the MSI and MSS groups were displayed using violin plots.

2.7 Statistical analysis

All statistical analyses were performed using IBM SPSS Statistics for Windows (version 26) and R (version 4.3.1, https://www.r-project.org). The normality of all quantitative data was tested using the Shapiro–Wilk test. Quantitative data following a normal distribution were described as mean ± standard deviation ($\bar{x} \pm s$), and group comparisons were performed using the independent samples t-test. Non-normally distributed data were expressed as median (M) and interquartile range (Q1, Q3), with group comparisons conducted using the Mann–Whitney *U* test. Categorical variables were described by frequency and percentage, and group comparisons were made using the Chi-square test or Fisher's exact test. For ranked data, group comparisons were performed using non-parametric rank-sum tests. The ROC curves of various models were plotted, and AUC values, sensitivity, specificity, and cut-off values were calculated to assess the efficacy of the models, where the cut-off values were obtained through the maximum Youden index. All statistical tests were two-tailed, and a $P < 0.05$ was considered statistically significant. Figures were generated using R software, Figdraw, and Origin software (version 2022).

3 Results

3.1 Patients and clinicopathologic data

A total of 63 CRC patients were included in this study [34 men (54.0%) and 29 women (46.0%)], with a mean age of 59.7 ± 13.4 years. Immunohistochemistry analysis revealed that 19 patients had MSI CRC, while 44 patients had MSS CRC. Compared to MSS CRC, MSI CRC is more commonly found in the right colon (26.3%), with a higher proportion showing no lymph node metastasis (LNM) (94.7%) and no serosal/mesangial layer invasion (63.2%). The predominant morphological classification is the raised type (42.1%), and an increased platelet count is also more frequently observed (42.1%). No statistically significant differences were found in other clinicopathological indicators between the two groups ($P > 0.05$) (Table 1). Univariate logistic regression analysis demonstrated that PLT and LNM are independent risk factors for predicting MSI in CRC ($P < 0.05$) (Table 2).

Differences in quantitative DCE-MRI parameters and ADC values between MSI and MSS groups.

A comparison of DCE-MRI quantitative parameters and ADC values between the MSI and MSS groups demonstrated that the MSI group had significantly lower K^{trans}, K_{ep}, and iAUC values than the MSS group ($P < 0.001$), while the ADC value in the MSI group was significantly higher than in the MSS group ($P = 0.016$). However, there was no statistically significant difference in V_e between the two groups ($P > 0.05$) (Table 1, Fig. 3).

3.2 Correlation analysis between imaging parameters and optimal clinical features

In patients with CRC, a negative correlation was observed between the K_{ep} vs. ADC value ($r = -0.258$, $P = 0.041$) and LNM vs. PLT ($r = -0.357$, $P = 0.004$); a positive correlation was observed between the Ktrans vs. iAUC ($r = 0.517$, $P < 0.001$) and LNM vs. iAUC ($r = 0.299$, $P = 0.017$). No significant correlations were found between the other imaging parameters and optimal clinical features included in the study ($P > 0.05$) (Fig. 4).

Table 1 Clinical and pathological data of 63 patients with colorectal cancer

Characteristic	Total (n = 63)	MSS (n = 44)	MSI (n = 19)	χ^2/Fisher/t/Z	*P*-value
Sex, n (%)				0.020	0.889
Male	34 (54.0)	24 (54.5)	10 (52.6)		
Female	29 (46.0)	20 (45.5)	9 (47.4)		
Age(y), n (%)				0.549	0.459
< 60	32 (50.8)	21 (47.7)	11 (57.9)		
≥ 60	31 (49.2)	23 (52.3)	8 (42.1)		
Tumor location, n (%)				12.774	0.002
Rectum	48 (76.2)	37 (84.1)	11 (57.9)		
Left colon	10 (15.9)	7 (15.9)	3 (15.8)		
Right colon	5 (7.9)	0 (0.0)	5 (26.3)		
LNM, n (%)				14.552	< 0.001
Positive	26 (41.3)	25 (56.8)	1 (5.3)		
Negative	37 (58.7)	19 (43.2)	18 (94.7)		
Serous/Mesangial layer invasion, n (%)				7.246	0.007
Positive	39 (61.9)	32 (72.7)	7 (36.8)		
Negative	24 (38.1)	12 (27.3)	12 (63.2)		
Degree of differentiation, n (%)				− 1.217	0.223
High	6 (9.5)	2 (4.5)	4 (21.1)		
Moderate	42 (66.7)	31 (70.5)	11 (57.9)		
Poor	15 (23.8)	11 (25.0)	4 (21.1)		
Morphological classification, n (%)				10.898	0.004
Ulcerative	39 (61.9)	28 (63.6)	11 (57.9)		
Protrude	13 (20.6)	5 (11.4)	8 (42.1)		
Infiltrate	11 (17.5)	11 (25.0)	0 (0.0)		
PLT(× 10^9/L), n (%)				− 3.159	0.002
100 ~ 300	49 (77.8)	39 (88.6)	10 (52.6)		
< 100	2 (3.2)	1 (2.3)	1 (5.3)		
> 300	12 (19.0)	4 (9.1)	8 (42.1)		
CEA (ng/mL), n (%)				0.490	0.484
< 5	39 (61.9)	26 (59.1)	13(68.4)		
≥ 5	24 (38.1)	18 (40.9)	6(31.6)		
CA19-9 (U/mL), n (%)				0.390	0.532
< 37	50 (79.4)	34 (77.3)	16 (84.2)		
≥ 37	13 (20.6)	10 (22.7)	3 (15.8)		
CA7-24 (ug/L), n (%)				0.603	0.437
< 6.7	42 (66.7)	28 (63.6)	14 (73.7)		
≥ 6.7	21 (33.3)	16 (36.4)	5 (26.3)		
HDL (mmol/L), n (%)				1.413	0.235
≤ 1.0	36 (57.1)	23 (52.3)	13 (68.4)		
> 1.0	27 (42.9)	21 (47.7)	6 (31.6)		
LDL (mmol/L), n (%)				–	1.000
< 3.4	56 (88.9)	39 (88.6)	17 (89.5)		
≥ 3.4	7 (11.1)	5 (11.4)	2 (10.5)		
K^{trans} [*M (Q1,Q3)*, min^{-1}]	0.227 (0.152–0.338)	0.241 (0.2, 0.4)	0.120 (0.1, 0.2)	−2.839	0.005
K_{ep} [*M (Q1,Q3)*, min^{-1}]	0.653(0.519–0.876)	0.700 (0.6, 1.0)	0.510 (0.4, 0.7)	− 3.759	< 0.001
V_e (Mean ± SD)	0.40 ± 0.16	0.41 ± 0.16	0.38 ± 0.16	−0.794	0.430
iAUC [M (Q1,Q3)]	12.385 (8.690–21.379)	15.997 (11.1, 28.0)	8.690 (6.4, 10.0)	− 3.534	< 0.001
ADC [*M (Q1,Q3)*, × 10^{-3} mm^2/s]	0.905 (0.848–0.990)	0.897 (0.8, 1.0)	0.960 (0.9, 1.1)	− 2.419	0.016

Table 1 (continued)

Data are numbers of patients, and data in parentheses are percentages. *CA19-9* carbohydrate antigen 19–9, *CA7-24* carbohydrate antigen 7–24, *CEA* carcinoembryonic antigen, *PLT* platelet, *HDL* high density lipoprotein, *LDL* low density lipoprotein, *LNM* Lymph node metastasis, *ADC* apparent diffusion coefficient, *MSI* microsatellite instability, *MSS* microsatellite stability

Table 2 Logistic regression analysis selected the optimal risk factors for preoperative prediction of MSI for colorectal cancer

Variables	Univariate logistic regression			
	β	OR	95%CI	*P*-value
PLT	2.054	7.800	1.949 ~ 31.216	0.004
LNM	3.165	23.684	2.900 ~ 193.442	0.003

95%CI 95% Confidence interval, *OR* Odds ratio, *β* regression coefficient, *PLT* platelet, *LNM* Lymph node metastasis

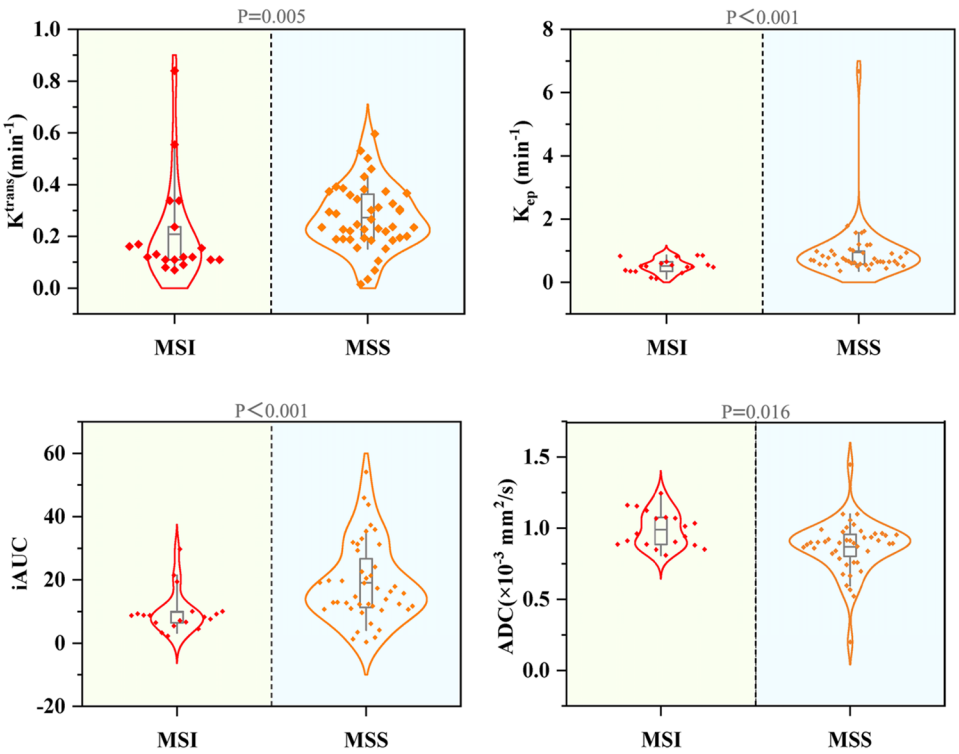

Fig. 3 The violin plots illustrate the comparison of DCE-MRI parameters and ADC values between the MSI and MSS groups. *MSS* microsatellite stability, *MSI* microsatellite instability, *ADC* apparent diffusion coefficient

3.3 Establishing a predictive model and nomogram

Univariate binary logistic regression was employed to develop the Clinical_model, K_{ep}_iAUC, K_{ep}_ADC, K_{ep}_iAUC_ADC, K^{trans}_K_{ep}, K^{trans}_iAUC, K^{trans}_ADC, K^{trans}_ADC_iAUC, K^{trans}_K_{ep}_ADC_iAUC, and the Combined_model. Backward stepwise logistic regression was used to identify factors associated with MSI. Ultimately, K^{trans}, K_{ep}, iAUC, ADC, PLT, and LNM were identified as independent predictors of MSI status and were subsequently incorporated into the nomogram construction (Fig. 5).

3.4 Predictive performance of nomogram and clinical application

The AUC, accuracy, sensitivity, specificity, threshold, and cutoff values for the 10 predictive models are presented in Table 3. Compared to the clinical model and other imaging parameter models, the combined model incorporating K^{trans}, K_{ep}, ADC, iAUC, and clinical features showed a slight improvement in performance [AUC, 0.951 (95% CI, 0.903–0.998)] (Fig. 6A). The performance comparison between Delong test models is shown in Table S2. Calibration curves and the

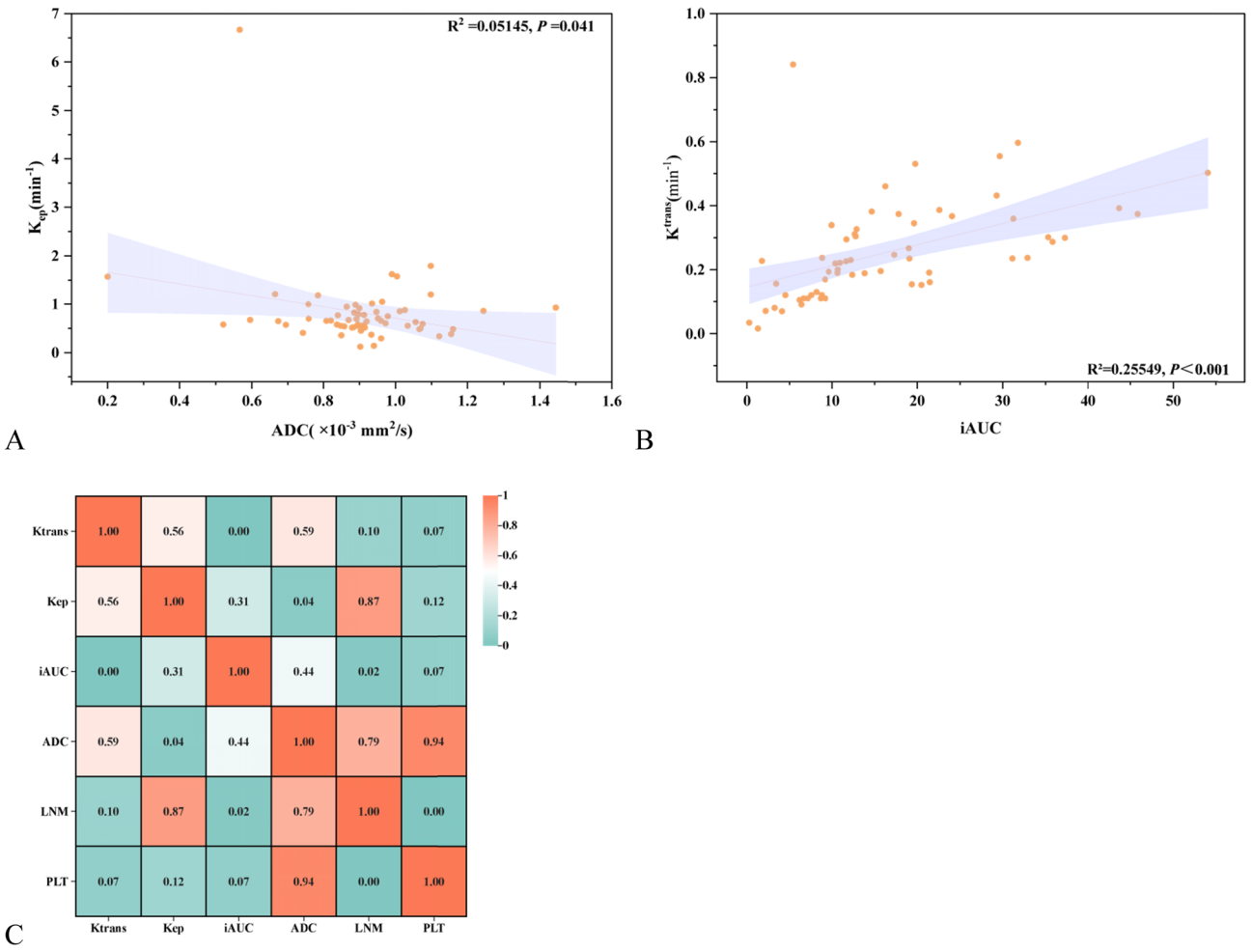

Fig. 4 Correlation analysis. **A** Correlation analysis between K_{ep} and ADC values; **B** correlation analysis between K^{trans} and iAUC; and **C** Heatmap of the correlation between the optimal clinical features, DCE-MRI parameters, and ADC values

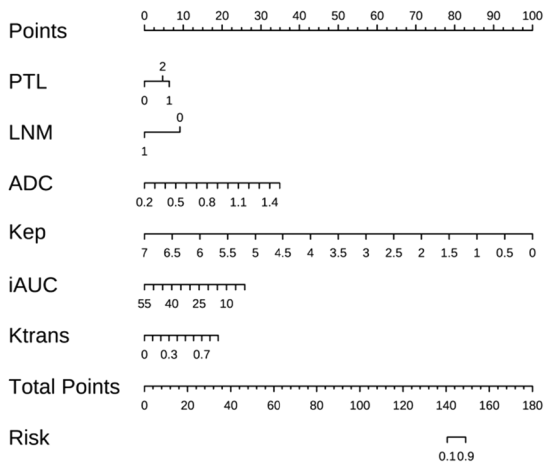

Fig. 5 Nomogram based on DCE-MRI parameters, ADC values and clinical features

Hosmer–Lemeshow H test confirmed that the model exhibited excellent goodness-of-fit ($P = 0.326$) (Fig. 6B). Furthermore, DCA and CIC analyses revealed that the combined model provides higher clinical utility and net benefit (Fig. 7).

Table 3 Comparison of ROC performance of different prediction models

Models	AUC	95%CI	Threshold value	Cut-off	Accuracy	Sensitivity	Specificity
Clinical_model	0.819	0.710 ~ 0.928	0.516	0.129	0.683	0.947	0.568
K^{ep}_iAUC	0.856	0.754 ~ 0.959	0.606	0.211	0.746	0.947	0.659
K^{ep}_ADC	0.850	0.746 ~ 0.955	0.600	0.382	0.825	0.737	0.864
K^{ep}_iAUC_ADC	0.897	0.815 ~ 0.979	0.653	0.399	0.841	0.789	0.864
K^{trans}_K_{ep}	0.800	0.677 ~ 0.923	0.548	0.414	0.810	0.684	0.864
K^{trans}_iAUC	0.781	0.651 ~ 0.911	0.683	0.377	0.841	0.842	0.841
K^{trans}_ADC	0.764	0.628 ~ 0.901	0.472	0.330	0.778	0.632	0.841
K^{trans}_ADC_iAUC	0.824	0.719 ~ 0.929	0.622	0.309	0.778	0.895	0.727
K^{trans}_K_{ep}_ADC_iAUC	0.897	0.821 ~ 0.974	0.652	0.168	0.778	0.947	0.705
Combined_model	0.951	0.903 ~ 0.998	0.818	0.131	0.873	1.000	0.818

AUC area under the curve, *95% CI* 95% confidence interval

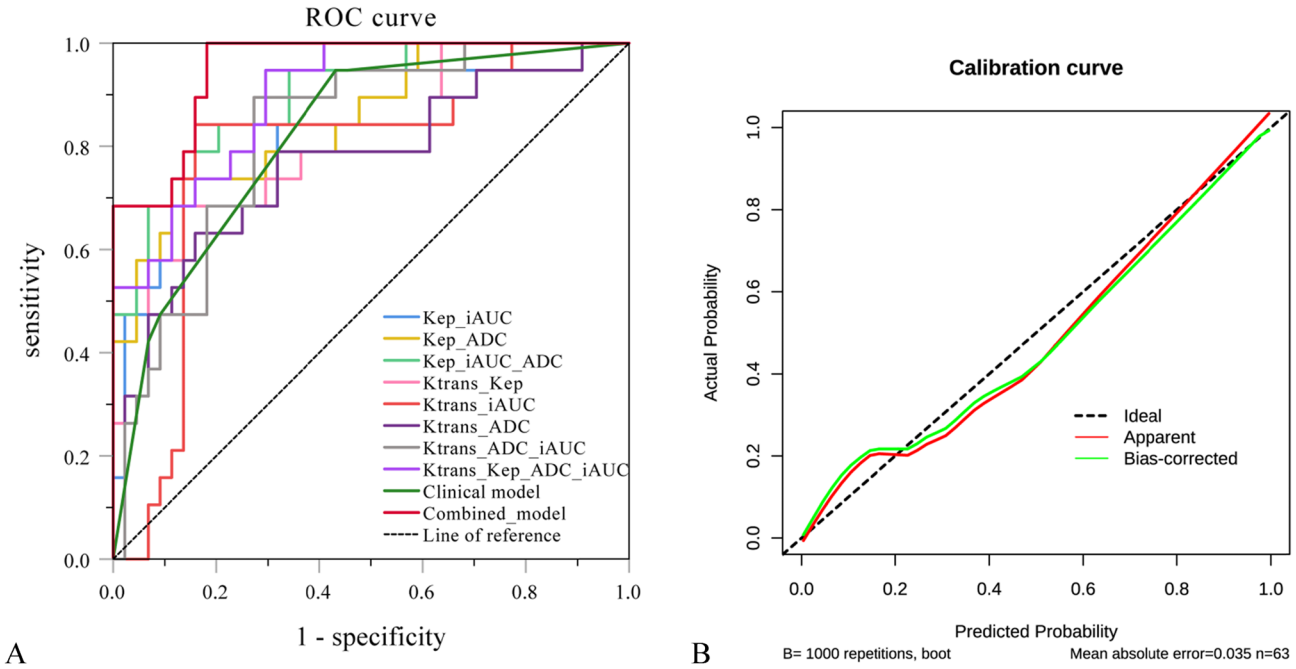

Fig. 6 Performance comparison of different models. **A** ROC curve of 10 predictive model performance comparison and **B** combination model calibration curve analysis

4 Discussion

In this study, the V_e parameter from DCE-MRI was excluded from further statistical analysis and model development due to its lack of statistical significance. Using K^{trans}, K_{ep}, iAUC, ADC values, PLT, and LNM, 10 predictive models were constructed. Our study demonstrates that the quantitative parameters from DCE-MRI and ADC values have potential utility in predicting MSI status in CRC patients. By incorporating DCE-MRI parameters, ADC values, and clinical characteristics, the nomogram model significantly improved the predictive performance for MSI status, achieving an AUC of 0.951. As this study is a single-center retrospective analysis, although the predictive performance of the model is promising, it remains in the exploratory phase. In the future, we plan to collect more prospective, multicenter data to further validate the reliability and generalizability of the model. While the current nomogram model requires further validation, it shows potential to provide valuable decision support for clinicians in clinical practice. Physicians can use the nomogram's indicators to perform individualized risk assessments for each CRC patient and predict their likelihood of MSI occurrence. At present, the gold standard for MSI evaluation remains pathological testing; however, tumor tissue biopsy is invasive,

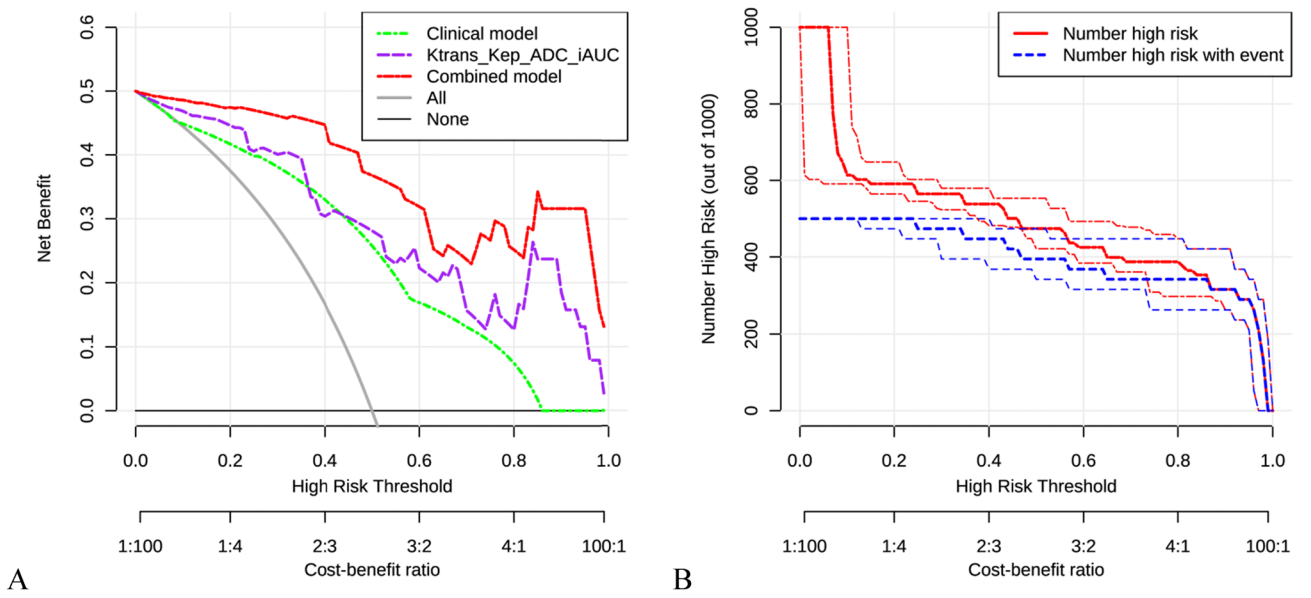

Fig. 7 Results of the decision analysis curve and clinical impact curve demonstrating excellent clinical application and net benefits of the combined model. **A** Comparison of decision analysis curves of three prediction models and **B** Clinical decision curve analysis of the combined model

and the results may be limited by the quantity and quality of the tissue sample. In the future, a radiogenomic nomogram model based on whole-tumor segmentation may offer a non-invasive method to evaluate MSI status, serving as a complementary tool to traditional pathology and addressing its limitations.

In recent years, radiogenomics, which integrates imaging, radiomics, genomics, and molecular characteristics, has emerged as a promising tool for non-invasive prediction of CRC genetic mutations and changes in the tumor microenvironment. Shin et al. [25] conducted a statistical analysis of MRI-derived features, including T stage, N stage, tumor location, tumor margins, enhancement pattern, T2 WI signal intensity, perirectal fat infiltration, and pelvic sidewall lymph node metastasis, in relation to KRAS mutation status. Their results revealed that the frequency of KRAS mutations was higher in N2 stage and polypoid tumors, and that KRAS-mutated tumors had longer lengths and larger axial-to-longitudinal size ratios. Additionally, Bodalal et al. [26] utilized radiomic features from T2 WI (TE75, TE300), DWI (b0, b10, b200, b800), and ADC to predict tumor hypoxia in CRC liver metastases. Different TE and b-values reflected the interaction between hemoglobin and oxygen-related magnetic molecules, as well as the restricted movement of water molecules in various hypoxic environments. Their study demonstrated that radiomic features from DWI b200 and ADC could significantly predict tumor hypoxia, providing important biological insights into the tumor microenvironment. As an important risk factor for CRC treatment and prognosis, the prediction of MSI is also crucial. Xing et al. [27] used MRI to predict MSI status in rectal cancer and found that the k-nearest neighbor model combining T2 WI and T1 CE achieved the best performance. Bodalal et al. [28] successfully predicted MSI status in CRC using radiomics from the venous phase of CT combined with clinical features. In comparison to previous studies, we utilized DCE-MRI parameters and ADC values to predict MSI status in CRC and found a good correlation between MRI quantitative parameters and MSI gene status. This indicates that a simple radiogenomic approach based on quantitative measurements has potential clinical value in genetic prediction.

DCE-MRI technology not only reflects the morphological characteristics of tumors but also provides biological information about the tumor perfusion microenvironment. Perfusion parameters based on DCE-MRI, such as K^{trans} and K_{ep}, can reflect the transfer of contrast agent between the capillaries and the extravascular extracellular space (EES), while iAUC is closely related to tumor blood perfusion levels and interstitial space, reflecting the tumor's blood supply and proliferation rate [20, 29]. This study found that compared to MSS CRC, MSI CRC had significantly lower K^{trans}, K_{ep}, and iAUC values. This difference may be attributed to the higher apoptosis-to-proliferation ratio, fewer actively proliferating tumor cells, reduced tumor microvessel density, and lower expression of vascular endothelial growth factor in MSI tumors [30–32]. Additionally, The ADC value serves as an indicator of the diffusion of extracellular water molecules; lower ADC values are associated with a greater degree of tumor malignancy [33]. This phenomenon occurs because malignant tumor cells exhibit rapid growth, leading to a reduction in extracellular space, which in turn restricts the movement of water

molecules [34]. In our study, the MSI group demonstrated higher ADC values ($P = 0.016$), further indicating the favorable biological behavior and prognosis associated with MSI CRC. Hong et al. [35]. Analyzed the MSI status of 29 patients with rectal cancer using DCE-MRI and found no significant correlation between MSI status and the semi-quantitative parameters of DCE-MRI. However, our study has distinct advantages. We included a larger cohort of patients and collected more comprehensive clinical data. By utilizing DCE-MRI parameters such as K^{trans}, K_{ep}, Ve, iAUC, and ADC values, we established ten predictive models that can accurately predict MSI in patients with CRC.

Previous studies have demonstrated that MSI CRC tends to occur in the right colon, with fewer lymph node metastases, often exhibiting significant "Crohn's like" lymphocyte infiltration and a higher lymph node count [36, 37], This could be related to the strong immune response associated with MSI CRC. The enlarged lymph nodes present significant challenges for preoperative evaluation of LNM, and excessive lymph node dissection during surgery is not beneficial for the long-term prognosis of patients [38]. In our study, we also observed that MSI CRC tends to occur in the right colon, with most cases showing no LNM and no serosal/mesangial layer invasion. These findings are consistent with previous studies, which suggest that MSI CRC is associated with better prognosis. Additionally, we identified PLT count in routine blood tests as an independent risk factor for predicting MSI. While the role of PLTs in hemostasis and vascular repair is well established, their involvement in tumor progression and immune evasion mechanisms has been less extensively studied. Tumor cells can evade immune surveillance by recruiting activated platelets and immune cells, encapsulating themselves into circulating tumor cells [39]. These mechanisms may offer potential avenues for developing antiplatelet therapies to inhibit tumor progression. Additionally, while some studies have suggested an association between tumor-associated markers and microsatellite status, others have found no such correlation. Our study demonstrated no significant association between tumor–associated markers and microsatellite status, which may be attributed to the small sample size.

This study has several limitations. First, retrospective single-center studies may introduce selection and information bias. The single-center design makes it difficult for the study results to fully reflect the clinical reality of patients from other centers, thereby limiting the external generalizability of the findings. Additionally, retrospective data collection may introduce potential temporal biases, making it challenging to fully control for certain confounding factors, which could impact the reliability of the conclusions. External validation is crucial to ensure the model's stability and reliability across different patient cohorts. In future research, we plan to adopt a multicenter, prospective design to enhance the representativeness of the findings and improve the model's broader applicability and external performance. Second, the relatively small sample size in this study may lead to model overfitting and limit its generalizability, particularly regarding its stability when applied to different patient populations. To overcome this limitation and improve the model's applicability, we plan to collect more prospective multicenter data in the future to further validate the robustness and stability of the model. Thirdly, although two experienced radiologists minimized bias in this study, a few measurement deviations caused by ROI were unavoidable. For small tumors, measuring DCE-MRI parameters and ADC values may be more challenging. In future studies, we will further optimize image segmentation techniques by incorporating more advanced automated segmentation tools to reduce bias from manual segmentation and improve the robustness of image analysis. Finally, the biological interpretability of imaging quantitative parameters in relation to genetic profiles remains challenging, requiring further research to uncover the potential links between radiogenomics, proteomics, and phenomics.

5 Conclusion

In conclusion, we proposed and developed a nomogram method that combines DCE-MRI perfusion parameters, ADC values, and clinical features to predict the MSI status of CRC patients. This model demonstrated good predictive potential and may assist clinicians in designing personalized treatment strategies and optimizing patient stratification and management for CRC.

Acknowledgements We would like to thank Zhaokun Wei and Xinli Li for their assistance with image acquisition and technical guidance. Additionally, we appreciate the efforts of the staff from the Radiology, Pathology, and colorectal surgery departments at Gansu Provincial Hospital for their contributions to the data collection for this study.

Author contributions Leping Peng and Wenting Ma designed the study and drafted the manuscript. Xiuling Zhang, Fan Zhang, Fang Ma, Kai Ai, Xiaomei Ma, Yingmei Jia, Hong Ou-Yang, Shengting Pei and Tao Wang were responsible for the collection and analysis of the experimental data. Yuanhui Zhu and Lili Wang revised the manuscript critically for important intellectual content. All authors read and approved the final manuscript.

Funding This work was supported by the Gansu Provincial Youth Science and Technology Fund Project (no. 20 JR5RA143), the Gansu Provincial Hospital Research Fund Project (no. 23GSSYF-4 and no. 23GSSYA-2), and Gansu Provincial Department of Education: Graduate Student "Innovation and Entrepreneurship" Project of Gansu University of Chinese Medicine, 2025 CXCY-071.

Data availability The data that support the findings of this study are not openly available due to reasons of sensitivity and are available from the corresponding author upon reasonable request. Data are located in controlled access data storage at Gansu Provincial Hospital.

Declarations

Ethics approval The study was approved by the Ethics Review Committee of Gansu Provincial Hospital (no. 2023-725). We confirm that all experiments were conducted in accordance with relevant guidelines and regulations. Although this study does not involve animal experiments, we have adhered to the ARRIVE guidelines (https://arriveguidelines.org) to ensure that the methodology is fully evaluable and reproducible.

Consent to participate All the authors have followed the applicable ethical standards to maintain the research integrity without any duplication, fraud or plagiarism issues. This study had the consent of all human participants, and all co-authors reviewed the manuscript and agreed to publish the study.

Consent for publication Not applicable.

Competing interests The authors declare that they are no competing interests in this study.

References

1. Bray F, Laversanne M, Sung H, Ferlay J, Siegel RL, Soerjomataram I, Jemal A. Global cancer statistics 2022: GLOBOCAN estimates of incidence and mortality worldwide for 36 cancers in 185 countries. CA Cancer J Clin. 2024;74:229–63.
2. Dekker E, Tanis PJ, Vleugels JLA, Kasi PM, Wallace MB. Colorectal cancer. Lancet. 2019;394:1467–80.
3. de Smedt L, Lemahieu J, Palmans S, Govaere O, Tousseyn T, van Cutsem E, Prenen H, Tejpar S, Spaepen M, Matthijs G, et al. Microsatellite instable vs stable colon carcinomas: analysis of tumour heterogeneity, inflammation and angiogenesis. Br J Cancer. 2015;113:500–9.
4. Sargent DJ, Marsoni S, Monges G, Thibodeau SN, Labianca R, Hamilton SR, French AJ, Kabat B, Foster NR, Torri V, et al. Defective mismatch repair as a predictive marker for lack of efficacy of fluorouracil-based adjuvant therapy in colon cancer. J Clin Oncol. 2010;28:3219–26.
5. Ribic CM, Sargent DJ, Moore MJ, Thibodeau SN, French AJ, Goldberg RM, Hamilton SR, Laurent-Puig P, Gryfe R, Shepherd LE, et al. Tumor microsatellite-instability status as a predictor of benefit from fluorouracil-based adjuvant chemotherapy for colon cancer. N Engl J Med. 2003;349:247–57.
6. Mi M, Weng S, Xu Z, Hu H, Wang Y, Yuan Y. CSCO guidelines for colorectal cancer version 2023: updates and insights. Chin J Cancer Res. 2023;35:233–8.
7. Benson AB, Venook AP, Al-Hawary MM, Arain MA, Chen YJ, Ciombor KK, Cohen S, Cooper HS, Deming D, Farkas L, et al. Colon cancer, version 2 2021, NCCN clinical practice guidelines in oncology. J Natl Compr Canc Netw. 2021;19:329–59.
8. Luchini C, Bibeau F, Ligtenberg MJL, Singh N, Nottegar A, Bosse T, Miller R, Riaz N, Douillard JY, Andre F, Scarpa A. ESMO recommendations on microsatellite instability testing for immunotherapy in cancer, and its relationship with PD-1/PD-L1 expression and tumour mutational burden: a systematic review-based approach. Ann Oncol. 2019;30:1232–43.
9. Yamamoto H, Watanabe Y, Arai H, Umemoto K, Tateishi K, Sunakawa Y. Microsatellite instability: a 2024 update. Cancer Sci. 2024;115:1738–48.
10. Yörüker EE, Holdenrieder S, Gezer U. Blood-based biomarkers for diagnosis, prognosis and treatment of colorectal cancer. Clin Chim Acta. 2016;455:26–32.
11. Li X, Huang W, Holmes JH. Dynamic contrast-enhanced (DCE) MRI. Magn Reson Imaging Clin N Am. 2024;32:47–61.
12. Delli Pizzi A, Caposiena D, Mastrodicasa D, Trebeschi S, Lambregts D, Rosa C, Cianci R, Seccia B, Sessa B, di Flamminio FM, et al. Tumor detectability and conspicuity comparison of standard b1000 and ultrahigh b2000 diffusion-weighted imaging in rectal cancer. Abdom Radiol (NY). 2019;44:3595–605.
13. Zhang K, Zheng Y, Huang H, Lei J. Preliminary study on predicting pathological staging and immunohistochemical markers of rectal cancer based on ADC histogram analysis. Acad Radiol. 2021;28(Suppl 1):S184-s191.
14. Ao W, Bao X, Mao G, Yang G, Wang J, Hu J. Value of apparent diffusion coefficient for assessing preoperative T staging of low rectal cancer and whether this is correlated With Ki-67 expression. Can Assoc Radiol J. 2020;71:5–11.
15. Lu ZH, Hu CH, Qian WX, Cao WH. Preoperative diffusion-weighted imaging value of rectal cancer: preoperative T staging and correlations with histological T stage. Clin Imaging. 2016;40:563–8.

16. Fontana G, Barcellini A, Boccuzzi D, Pecorilla M, Loap P, Cobianchi L, Vitolo V, Fiore MR, Vai A, Baroni G, et al. Role of diffusion-weighted MRI in recurrent rectal cancer treated with carbon ion radiotherapy. Future Oncol. 2022;18:2403–12.
17. Liu Z, Zhu L, Liu Y, Huang X, Wang C, Yu Y. Predictive value of apparent diffusion coefficient for neoadjuvant chemotherapy in locally advanced colorectal cancer patients. J Gastrointest Oncol. 2023;14:789–97.
18. Pikūnienė I, Saladžinskas Ž, Basevičius A, Strakšytė V, Žilinskas J, Ambrazienė R. MRI evaluation of rectal cancer lymph node staging using apparent diffusion coefficient. Cureus. 2023;15: e45002.
19. Yuan Y, Chen XL, Li ZL, Chen GW, Liu H, Liu YS, Pang MH, Liu SY, Pu H, Li H. The application of apparent diffusion coefficients derived from intratumoral and peritumoral zones for assessing pathologic prognostic factors in rectal cancer. Eur Radiol. 2022;32:5106–18.
20. Ao W, Zhang X, Yao X, Zhu X, Deng S, Feng J. Preoperative prediction of extramural venous invasion in rectal cancer by dynamic contrast-enhanced and diffusion weighted MRI: a preliminary study. BMC Med Imaging. 2022;22:78.
21. Bodalal Z, Trebeschi S, Nguyen-Kim TDL, Schats W, Beets-Tan R. Radiogenomics: bridging imaging and genomics. Abdom Radiol (NY). 2019;44:1960–84.
22. Cai Z, Xu Z, Chen Y, Zhang R, Guo B, Chen H, Ouyang F, Chen X, Chen X, Liu D, et al. Multiparametric MRI subregion radiomics for preoperative assessment of high-risk subregions in microsatellite instability of rectal cancer patients: a multicenter study. Int J Surg. 2024;110:4310–9.
23. Li Z, Zhang J, Zhong Q, Feng Z, Shi Y, Xu L, Zhang R, Yu F, Lv B, Yang T, et al. Development and external validation of a multiparametric MRI-based radiomics model for preoperative prediction of microsatellite instability status in rectal cancer: a retrospective multicenter study. Eur Radiol. 2023;33:1835–43.
24. Zhang P, Wang A, Bian C, Zhang J, Jiang C, Zhou H. Evaluation of mismatch-repair and microsatellite-instability status in a Chinese colorectal cancer Cohort. Asian J Surg. 2024;47:959–67.
25. Shin YR, Kim KA, Im S, Hwang SS, Kim K. Prediction of KRAS mutation in rectal cancer using MRI. Anticancer Res. 2016;36:4799–804.
26. Bodalal Z, Bogveradze N, Ter Beek LC, van den Berg JG, Sanders J, Hofland I, Trebeschi S, Groot Lipman KBW, Storck K, Hong EK, et al. Radiomic signatures from T2W and DWI MRI are predictive of tumour hypoxia in colorectal liver metastases. Insights Imaging. 2023;14:133.
27. Xing X, Li D, Peng J, Shu Z, Zhang Y, Song Q. A combinatorial MRI sequence-based radiomics model for preoperative prediction of microsatellite instability status in rectal cancer. Sci Rep. 2024;14:11760.
28. Bodalal Z, Hong EK, Trebeschi S, Kurilova I, Landolfi F, Bogveradze N, Castagnoli F, Randon G, Snaebjornsson P, Pietrantonio F, et al. Non-invasive CT radiomic biomarkers predict microsatellite stability status in colorectal cancer: a multicenter validation study. Eur Radiol Exp. 2024;8:98.
29. Krishan S, Patel A, Sud R, Puri R, Vaid A, Lipi L, Kataria T. Rectal perfusion parameters normalised to tumour-free rectal wall can predict response to neoadjuvant chemoradiotherapy. Clin Radiol. 2018;73:151–7.
30. Toh J, Chapuis PH, Bokey L, Chan C, Spring KJ, Dent OF. Competing risks analysis of microsatellite instability as a prognostic factor in colorectal cancer. Br J Surg. 2017;104:1250–9.
31. Wynter CV, Simms LA, Buttenshaw RL, Biden KG, Young J, Leggett BA, Conrad RJ, Schoch EM, Jass JR, Praga Pillay S. Angiogenic factor VEGF is decreased in human colorectal neoplasms showing DNA microsatellite instability. J Pathol. 1999;189:319–25.
32. Miyamoto N, Yamamoto H, Taniguchi H, Miyamoto C, Oki M, Adachi Y, Imai K, Shinomura Y. Differential expression of angiogenesis-related genes in human gastric cancers with and those without high-frequency microsatellite instability. Cancer Lett. 2007;254:42–53.
33. Gürses B, Böge M, Altınmakas E, Balık E. Multiparametric MRI in rectal cancer. Diagn Interv Radiol. 2019;25:175–82.
34. Yacheva A, Dardanov D, Zlatareva D. The multipurpose usage of diffusion-weighted MRI in rectal cancer. Medicina (Kaunas). 2023;59:2162.
35. Hong HS, Kim SH, Park HJ, Park MS, Kim KW, Kim WH, Kim NK, Lee JM, Cho HJ. Correlations of dynamic contrast-enhanced magnetic resonance imaging with morphologic, angiogenic, and molecular prognostic factors in rectal cancer. Yonsei Med J. 2013;54:123–30.
36. Belt EJ, te Velde EA, Krijgsman O, Brosens RP, Tijssen M, van Essen HF, Stockmann HB, Bril H, Carvalho B, Ylstra B, et al. High lymph node yield is related to microsatellite instability in colon cancer. Ann Surg Oncol. 2012;19:1222–30.
37. Kim YT, Min JH, Choi KH, Kim H. Colon cancer microsatellite instability influences computed tomography assessment of regional lymph node morphology and diagnostic performance. Eur J Radiol. 2022;154: 110396.
38. Inamori K, Togashi Y, Fukuoka S, Akagi K, Ogasawara K, Irie T, Motooka D, Kobayashi Y, Sugiyama D, Kojima M, et al. Importance of lymph node immune responses in MSI-H/dMMR colorectal cancer. JCI Insight. 2021;6:137365.
39. Wang L, Wang X, Guo E, Mao X, Miao S. Emerging roles of platelets in cancer biology and their potential as therapeutic targets. Front Oncol. 2022;12: 939089.